Analytical Methods

Accepted Manuscript

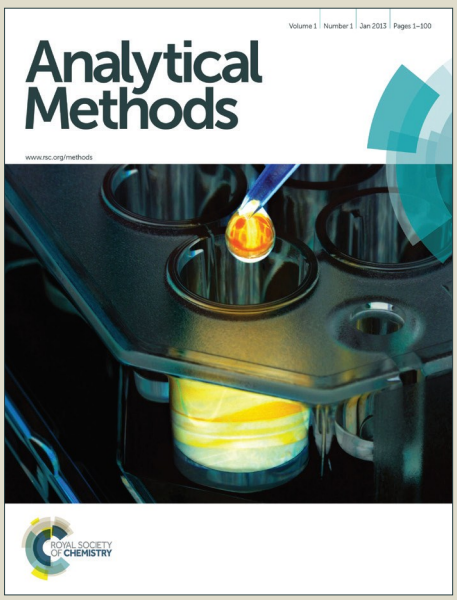

This is an *Accepted Manuscript*, which has been through the Royal Society of Chemistry peer review process and has been accepted for publication.

Accepted Manuscripts are published online shortly after acceptance, before technical editing, formatting and proof reading. Using this free service, authors can make their results available to the community, in citable form, before we publish the edited article. We will replace this *Accepted Manuscript* with the edited and formatted *Advance Article* as soon as it is available.

You can find more information about *Accepted Manuscripts* in the Information for Authors.

Please note that technical editing may introduce minor changes to the text and/or graphics, which may alter content. The journal's standard Terms & Conditions and the Ethical guidelines still apply. In no event shall the Royal Society of Chemistry be held responsible for any errors or omissions in this *Accepted Manuscript* or any consequences arising from the use of any information it contains.

ROYAL SOCIETY OF CHEMISTRY

www.rsc.org/methods

composites[15]. Thus, metal nanoparticles-decorated graphene composites have become the focus of research for scientists in recent years. Generally, an efficient method for the large-scale production of graphene in low cost is the chemical reduction of exfoliated graphene oxide (GO). However, the reagents used for the reduction of GO usually are either highly toxic like hydrazine, dimethylhydrazine, hydroquinone and $NaBH_4$, or time consuming such as sugar, ascorbic acid, and dopamine[16, 17]. Furthermore, as-prepared graphene by this way usually shows poor dispersibility in aqueous solution due to agglomerate irreversibly through van der Waals interactions[18]. Recently, a satisfactory result has been achieved by using Poly(diallyldimethylammonium chloride) (PDDA), a positively charged polyelectrolyte, as a dispersing agent and a stabilizer to prepare graphene from exfoliated GO[19, 20]. In view of these aspects, the methods of developing the room temperature eco-friendly, simple operation and easy to disperse metal nanoparticle-rGO hybrid materials are expected to create more opportunity for biological sensing applications.

Herein, we fabricated a kind of hydrosoluble metal nanoparticle-rGO hybrid material by the in situ reduction of both GO and Pt (Ⅳ) in acidic solution using metallic Zn in the presence of PDDA. This method is not only simple and cost effective, but also eco-friendly and short time-consuming. The obtained Pt-PDDA-rGO hybrid material was used for constructing a sensitive amperometric sensing platform to detect the H_2O_2 at low applied potential. The result demonstrates that the non-enzymatic biosensor exhibits excellent electrocatalytic response to H_2O_2, along with high sensitivity and wide linear range.

2 Experimental

2.1 Apparatus

Transmission electron microscope (TEM) image was taken with a JEM-3010 transmission electron microscope (JEOL Co., Ltd., Japan). FT-IR spectra of KBr powder-pressed pellets were recorded on a Fourier transform-infrared (FT-IR) spectrophotometer (USA). UV-Vis spectra were obtained from a UV-Vis spectrometer (Perkin Elmer, USA). Electrochemical measurements were performed on a CHI660C electrochemical workstation (Austin, TX, USA) with conventional three-electrode system. Electrochemical impedance spectroscopy (EIS) experiments were performed on Multi-potentiostat (VMP2, Princeton Applied Research, USA). A bare or modified glassy carbon electrode (GCE, 3mm in diameter) was employed as working electrode. A platinum wire electrode and a saturated calomel electrode (SCE) were served as the auxiliary and reference electrode, respectively. All potentials given in this paper were referred to the SCE. Before each electrochemical measurement, solutions were thoroughly deoxygenated by bubbling nitrogen through the solution for at least 20min to remove dissolved oxygen.

2.2 Reagents

Graphite (99.99% SP-1, Bay carbon) with average particle size of 45 μm was obtained from Shanghai Chemical Reagent (Shanghai, China). Hydrogen peroxide solution (30wt%) was purchased from Beijing Chemical Reagent (Beijing, China), hexachloroplatinic acid ($H_2PtCl_6 \bullet 6H_2O$), poly(diallyldimethylammonium chloride) solution (PDDA, Mw<100,000, 35wt% in water) and Zn powders (≥99%) were purchased from Aladdin. Phosphate buffer solution (PBS, 0.1M, pH 7.0) was prepared by mixing suitable amounts of 0.2 M NaH_2PO_4/Na_2HPO_4. All other chemicals used in this investigation were of analytical grade, and all the solutions used in this investigation were prepared with Millipore water (Milli-Q system).

2.3 Synthesis of GO and Pt-PDDA-rGO

GO was synthesized according to modified Hummer's method[21] by the exfoliation of graphite. Briefly, 46 mL concentrated H_2SO_4 was slowly added to a mixture of graphite powder (2 g) and $NaNO_3$ (1 g) in a 250 mL three-necked flask at 0 °C. Solid $KMnO_4$ (6 g) was gradually added to the reaction mixture at <10 °C and the mixture was stirred continuously for 2 h at room temperature. Water (150 mL) was slowly added to the mixture until the temperature rised to 85 °C and the stirring was continued for another 30 min. Then 6 mL 30% H_2O_2 solution was added to the reaction vessel until the gas evolution was ceased. The resulting mixture was centrifuged in an ultra-centrifuge to remove the residual unexfoliated graphite and oxidizing agents. The residue was then washed repeatedly with 5% HCl solution until the sulfate ions in the washing solution were completely removed. The residue obtained after repeated washing was further washed with copious amount of Millipore water and dried in vacuum to get the yellow brown solid of graphite oxide. Then graphite oxide was dispersed in water by ultrasonication for 1 h, followed by centrifugation at 4000 rpm for 25 min to remove any unexfoliated products, the supernatant solution was centrifugatied at 11000 rpm for 25 min and dried in vacuum to get graphene oxide(GO).

The Pt-PDDA-rGO hybrid material was synthesized by the in situ reduction of both GO and Pt (Ⅳ) in acidic solution using Zn[22, 23], and PDDA served as the dispersing and stabilizing agents. Firstly, 6 mL of 0.2 wt% PDDA solution, 1 g of metallic Zn powders were slowly added into the 5 mL of 1 mg/mL GO dispersion to make a homogenous suspension by 5 minutes sonication. Subsequently, we added 10 mL 5 M H_2SO_4 along with 2 mL 0.01 M H_2PtCl_6 solution into the reaction mixture and allowed the reaction to proceed for 1 h. The excess Zn was removed by adding corresponding acid solution. Finally, the black colored Pt-PDDA-rGO hybrid material was collected by centrifugation at 13,000 rpm for 15 min and further washed with water several times to remove the unreacted metalions and dried at 60 °C for 12 h in a vacuum oven. All the reactions were carried out in room temperature and ambient pressure. Similarly, we prepared PDDA-rGO, Pt-rGO, Pt-PDDA by the same procedure to compare with the Pt-PDDA-rGO.

2.4 Fabrication of the H_2O_2 sensor

Before modification, the bare GCE was polished with 1.0, 0.3 and 0.05μm alumina slurry to a mirror-like, respectively, followed by rinsing thoroughly with doubly distilled water. For preparation of the electrochemical sensor, Pt-PDDA-rGO was firstly dispersed in water under sonication for 5 min to obtain a stable black suspension. Then 5μL of 1mg/mL suspension was dropped onto the GCE surface and dried in air. Then the modified electrode was obtained.

2.5 Blood collection and handling

All human serum samples were obtained from voluntary individuals in Northwest Normal University Hospital (Lanzhou, China). All experiments were performed in compliance with the relevant laws and institutional guidelines of the Ethics Committee of the Hospital, and informed consent was obtained from the voluntary individuals who provided the human samples.

3 Results and discussion

3.1 Synthesis of Pt-rGO-PDDA hybrid material

The hybrid material was synthesized by one-pot approach at room temperature using metallic Zn and mineral acid, as shown in the Scheme.1. There are four prominent highlights about this reaction. Firstly, metallic Zn and mineral acid plays a dual role in the reaction medium. One is the reduction of GO by generated hydrogen and the other is deposition of Pt nanoparticles on rGO by galvanic replacement reaction between Zn and $PtCl_6^{2-}$ [24]. Secondly, the reaction is time-saving and high efficiency because it just takes one hour to make $PtCl_6^{2-}$ and GO reduce to Pt and rGO, respectively. Thirdly, this method is green and environmental friendly since it doesn't use the harmful chemical reductants such as hydrazine hydrate and sodium borohydride. Finally, the introduction of PDDA prevents the aggregation of both graphene sheets and the PtNPs, and increases the dispersion of the Pt nanoparticles-rGO hybrid materials in water, which was proved by the photos of different synthetic materials shown in Fig.S1.

To examine the water-dispersible performance of the as-prepared Pt-PDDA-rGO material, the sample was dispersed in distilled water at a concentration of 1 mg mL^{-1}. After mild sonication, Pt-PDDA-rGO formed a very stable dispersion in water that was stable for more than six months. In addition, we have also measured the UV-vis absorbance spectra of the Pt-PDDA-rGO aqueous solution at different concentrations. As shown in Fig.S2, the maximum absorption peak of Pt-PDDA-rGO aqueous solution appeared at 263 nm, and the peak increased with the increase of the concentration. The inset shows a linear relationship exists between the absorbance and the concentration of Pt-PDDA-rGO. It is evident that the absorbance values of Pt-PDDA-rGO aqueous solutions at different concentrations obey Beer's law, and the molar absorption coefficient (ε) was calculated to be 26.50 ml mg^{-1} cm^{-1}. The maximum dispersibility of Pt-PDDA-rGO hybrid material in water was determined to be 1.24 mg ml^{-1}. This is in good agreement with the water-dispersible graphene prepared by Wang et al[25]. The high ε value of the aqueous dispersion of Pt-PDDA-rGO indicates that it is highly dispersible in water.

Scheme.1

3.2 Characterization of Pt-PDDA-rGO

3.2.1 Morphological and structural characterization

The detailed morphology and structure of the as-generated GO, PDDA-rGO and Pt -PDDA-rGO were examined by TEM, EDS, FTIR and UV-Vis. The layer structure and crystalline nature of the hybrid material were characterized first by TEM as shown in Fig.1. The pristine GO (A) has a hyaline surface with wrinkled textures, while the PDDA-rGO (B) sheets exhibit more wrinkled and crumpling features than GO, which are attributed to the distortion of carbon structure caused by the remnants of the epoxy reaction[26]. Fig.1C shows the Pt nanoparticles are well formed and evenly dispersed on the surface of rGO despite of some slight aggregation. Moreover, the high resolution TEM image (Fig. 1D) further shows that the size of Pt nanoparticles ranges from 5 to 10 nm, and the inset of Fig. 1D displays PtNPs have a lattice spacing of 0.225 nm, corresponding to the Pt (111) plane[27]. The concentric rings consisting of distinct spots can be seen from the selected area electron diffraction (SAED) pattern (Fig. 1E), which are a result of many small single crystals and suggests the crystalline nature of Pt nanoparticles[28]. In addition, the energy dispersive spectrometry (EDS) spectrum exhibits strong peaks of Pt, C and N, suggesting the formation of Pt-PDDA-rGO.

Next, the composition and structure of the hybrid material were analyzed and identified by using FTIR spectrum. As shown in Fig.S3, GO has a typical peak at 1732 cm^{-1} due to the skeletal vibration of C=O, suggesting the existence of oxygen functionalities on the GO surface[29]. In addition, the spectrum of GO also has other characteristic peaks, namely, O-H stretching (3429 cm^{-1}), O-H deformation vibrations (1400 cm^{-1}), and alkoxy C-O-C (1070 cm^{-1}). For PDDA-rGO, the characteristic absorption bands of the oxygenic groups decreased, confirming the reduction of GO. Moreover, the spectrum of PDDA-rGO exhibits typical peaks at 2924 cm^{-1} (CH_n), 1463 cm^{-1} (CH_2), and 1113 cm^{-1} (C-N) which are corresponding to the characteristic bands of PDDA, indicating the presence of PDDA in graphene nanosheets[30]. The Pt-PDDA-rGO curve is similar to the PDDA-rGO curve, but the peak intensities of the former are obviously weaker than the latter. The reason may be that the presence of $PtCl_6^{2-}$ makes the reduction reaction more thoroughly.

Finally, UV-vis spectroscopy was also utilized to characterize the Pt-PDDA-rGO hybrid material. In Fig.S4, the UV-vis spectrum of GO shows two bands at ~234 and ~302 nm, corresponding to the π-π* transition of the aromatic C-C and the n-π* transition of the C=O bond, respectively[31]. While for the PDDA-rGO, the absorption peak at 234 nm was shifted to 269 nm. At the same time, the shoulder peak at 302 nm was disappeared, indicating that GO has been completely reduced. Compared with PDDA-rGO, the maximum absorption peak

position of Pt-PDDA-rGO has hardly shifted, suggesting that Pt almost has no influence to the peak position[32]. By all accounts above, we can conclude that the Pt-PDDA-rGO has been successfully synthesized.

Fig.1

3.2.2 Electrochemical characterization of Pt-PDDA-rGO

The charge transfer property of Pt-PDDA-rGO modified electrode was characterized by using electrochemical method. Fig.2 showed the cyclic voltammograms (CVs) obtained at bare GCE(a), PDDA-rGO/GCE(b), and Pt-PDDA-rGO/GCE (c) in the 10 mM $Ru(NH_3)_6^{3+}$ and 0.1 M KCl solution at 50 mV/s. A pair of redox peaks was observed in each CV, which was ascribed to the redox of $Ru(NH_3)_6^{3+}$. After modified with PDDA-rGO, the anodic peak and cathodic peak (curve b) both increased apparently because of good electrical conductivity and large specific surface area of rGO. While the Pt-PDDA-rGO modified electrode was scanned in the same solution, the peak current (curve c) decreased a lot compared with the PDDA-rGO/GCE. The reason, we think, may be ascribed to the quantum size effect of nanoparticles. According to Kubo theory[33], the smaller of Pt nanoparticle, the more obvious of quantum size effect, and the poor conductivity it has.

Fig.2

In order to further illustrate the reasons mentioned above, we have measured the electrochemical impedance spectroscopy (EIS) of different electrodes, as shown in Fig.S5. By using $[Fe(CN)_6]^{3-/4-}$ as the electrochemical probe, the Nyquist plots of different electrodes were obtained and the inset is the fits of equivalent circuit. The impedance spectra of the bare GCE (Fig.S5a) consisted of a semicircle (Ret: 110Ω) with an almost straight tail line, the semicircle portion at higher frequencies corresponding to the electron transfer-limited process and the linear part at lower frequency range representing the diffusion limited process. When the PDDA-rGO modified the surface of GCE electrode, the diameter of the high frequency semicircle was significantly reduced to an almost straight line as shown in Fig.S5b, which further confirmed that the rGO effectively enhanced the conductivity of the modified electrode. While for the Pt-PDDA-rGO/GCE (Fig.S5c), the electron transfer resistance increased to about 26Ω compared with PDDA-rGO, illustrating that the conductivity of the modified electrode decreased after loading PtNPs. Therefore, the quantum size effect at Pt-PDDA-rGO/GCE is clearly, resulting in the conductivity decrease. The result is in agreement with the CV experiment as shown in Fig.2.

Cyclic voltammetry (CV) is also a common and convenient method to characterize the catalytic activities of the as-prepared electrodes. Fig.3 represented CVs of various modified electrodes in N_2-saturated 0.2 M PBS (pH 7.0). Compared with bare GCE (a) and PDDA-rGO/GCE (b), a cathodic peak at 0.051 V was obtained on the Pt-rGO/GCE (c), Pt-PDDA/GCE (d), and Pt-PDDA-rGO /GCE (e), respectively, which was attributed to the reduction of platinum oxide, also proving the existence of PtNPs on the modified electrode. It was noticeable that the peak current of curve e was much higher than that of curve c and d, illustrating great amount of PtNPs loaded on the surface of PDDA-rGO. Generally, the specific surface area and numbers of active sites on the surface can significantly affect the catalytic activity of the modified electrode. In a proper range, the greater loading of PtNPs, the more activity sites on surface, and the higher catalytic activity it has. So the load of PtNPs is beneficial to improve the catalytic performance of modified materials.

Fig.3

3.3 Electrochemical response of H_2O_2 at the Pt-PDDA-rGO/GCE

Fig.4

The electrochemical responses of H_2O_2 at different electrodes were demonstrated in Fig.4. It was obviously seen that the responses of H_2O_2 were quite weak at bare GCE (curve a) and PDDA-rGO/GCE (curve b), indicating that the two electrodes have no appreciable electrocatalytic activity toward the H_2O_2 reduction. In contrast, Pt nanoparticles modified electrodes exhibited the remarkable increases of the reduction current as shown in curves c-e. The reductive peak of the Pt-rGO/GCE (c) was broad and not big enough, which was due to the poor dispersion and tendentious agglomeration for the modified material without PDDA. However, the Pt-PDDA-rGO/GCE(e) produced excellent response signals with the much higher catalytic current and more positive reduction potential (0.051 V) than the Pt-PDDA/GCE(d), which further evidenced that rGO provided a large specific surface used for the load of PtNPs, and suggested the excellent catalytic activity of PtNPs for reduction of H_2O_2.

The catalytic mechanism of Pt-PDDA-rGO modified electrodes towards H_2O_2 was also discussed. As shown in inset of Fig. 4, a reduction peak (curve a) was observed on modified electrode in the PBS without H_2O_2, which should be attributed to the reduction of platinum oxide itself [34]. After adding H_2O_2, the reduction peak current (curve b) increased dramatically, indicating that H_2O_2 promoted the electrocatalytic reduction of platinum oxide on the surface of the electrode. This observation can be explained with the electrocatalytic reduction mechanism of H_2O_2 on the modified electrode as following reactions (1) and (2). According to the reactions, the dissociative adsorption of H_2O_2 on the platinum surface increases the production of platinum oxide (Eq. (1)). Meanwhile, the increase of platinum oxide further promotes its electrochemical reduction (Eq. (2)). Thus, the more production of platinum oxide, the greater reduction peak current of platinum it has, as shown in curve b in the inset of Fig. 4. This is similar to the results reported in previous

literature[35]. Therefore, the proposed Pt-PDDA-rGO modified electrode may realize the determination to H_2O_2.

$$2Pt + H_2O_2 \xrightarrow{k_1} 2Pt - OH \quad (1)$$

$$Pt - OH + H^+ + e^- \xrightarrow{k_2} Pt + H_2O \quad (2)$$

3.4 Performance of the hydrogen peroxide sensor

3.4.1 Amperometric response and calibration curve

To assess the amperometric response of the Pt-PDDA-rGO/GCE for hydrogen peroxide reduction, amperometric detection was performed with the successive addition of H_2O_2 to N_2-saturated 0.2 M PBS (pH 7.0) at an applied potential 0 V. As shown in Fig.5, the current responses of the sensor increased along with H_2O_2 concentrations. The response to logarithm of the H_2O_2 concentration showed linear range from 1.0×10^{-9} to 8.6×10^{-6} M (inset of Fig. 5B), and the linear regression equation was Ip(μA)=0.1692lg[H_2O_2]+2.8090 with a correlation coefficient of 0.9940. Another linear relationship could be established between the peak currents and the concentrations of H_2O_2 in the range from 1.8×10^{-5} to 1.4×10^{-3} M (Fig.5D), and the linear regression equation was Ip(μA)=0.0044[H_2O_2](μM)+1.9427 with a correlation coefficient of 0.9999. The detection limit of as-prepared electrochemical sensor was calculated to be 3.4×10^{-10} mol/L according to the formula, 3σ/b [36], where σ is the standard deviation of three measures of the blank and b is the slope of the calibration curve.

Table 1 summarizes this sensor performance based on Pt-PDDA-rGO hybrid material and other relevant sensor materials collected from literatures. We found that the performance of the proposed sensor was better than other non-enzymatic H_2O_2 sensors, particularly the lower LOD. The result indicated that the high electrocatalytic efficiency of Pt-PDDA-rGO sensor was attributed to the large quantities of Pt nanoparticles, which were well dispersed on the rGO surface.

Fig.5

Table 1

3.4.2 Selectivity, reproducibility and stability of the H2O2 sensor

The possible interferences from some co-existing electroactive compounds in real samples such as dopamine (DA), uric acid (UA) and ascorbic acid (AA) were assessed in order to investigate the selectivity of the developed sensor. Fig.6 displayed the amperometric i-t response of the Pt-PDDA-rGO/GCE upon the successive addition of H_2O_2, UA, DA, AA and H_2O_2 (0.1mM, respectively) to 0.2 M N_2-saturated PBS (pH 7.0) at an applied potential of 0 V with stirring condition. The two electrochemical signals derived from H_2O_2 were basically identical and the responses caused by UA, DA and AA could be negligible. It indicates that the proposed non-enzymatic electrode can be employed in the selective and sensitive detection of H_2O_2 in the presence of these common physiological materials.

The reproducibility and stability are also important parameters to evaluate the performance of the sensor. The reproducibility of the modified electrode was estimated from the response to 50 μM H_2O_2 at five different H_2O_2 electrodes in Fig.S6, and an acceptable relative standard deviation (RSD) of 3.75% was acquired. Moreover, after 200 segments continuous CV scanning of the modified electrode in N_2-saturated 0.2 M PBS (pH 7.0) containing 0.1 mM H_2O_2 at 50 mV/s, it was still able to get 92.36% of the original value as shown in Fig.S7. The results suggested the excellent reproducibility and the stability of the sensor.

Fig.6

3.4.3 Real sample analysis

The sensor was applied for the determination of H_2O_2 in 1% human serum samples utilizing standard addition method. The concentration of H_2O_2 in serum samples was determined to be 15.58 nM (n=3) by chronamperometry measurement, and the recoveries of H_2O_2 samples with concentrations of 10 nM (sample 2), 20 nM (sample 3), and 30 nM (sample 4) were obtained in Table 2. These results were consistent with previously report[46], and showed that the sensor has a potential in detection of hydrogen peroxide directly in biological samples.

Table 2

4 Conclusions

In summary, we successfully synthesized the Pt-PDDA-rGO hybrid material by a green approach where metallic Zn was chosen as the reductant and PDDA as a stabilizer and dispersant. The results indicate that the hybrid material can greatly enhance the electrocatalytic activity towards the reduction of H_2O_2 because of the synergistic effect of the Pt nanoparticles and rGO. The constructed Pt-PDDA-rGO sensor exhibits an ultra-low detection limit, wide linear range, good reproducibility, long-term stability and satisfactory anti-interference ability, which make it very promising for detection of H_2O_2 in biological systems.

Acknowledgements

This work was supported by the National Natural Science Foundation of China (Nos. 21245004 and 20875077), and Program for Chang Jiang Scholars and Innovative Research Team, Ministry of Education, China (Grant no. IRT1283).

References

1 M. Ahmad, C. Pan, L. Gan, Z. Nawaz and J. Zhu, *J. Phys. Chem. C*, 2009, **114**, 243-250.
2 W. Chen, S. Cai, Q. Q. Ren, W. Wen and Y. D. Zhao, *Analyst*, 2012, **137**, 49-58.
3 F. Pagliari, C. Mandoli, G. Forte, E. Magnani, S. Pagliari, G. Nardone, S. Licoccia, M. Minieri, P. Di Nardo and E. Traversa, *ACS Nano.*, 2012, **6**, 3767-3775.
4 Y. Zhang, X. Bai, X. Wang, K. K. Shiu, Y. Zhu and H. Jiang, *Anal. Chem.*, 2014, **86**, 9459-9465.
5 P. Nagaraja, A. Shivakumar and A. K. Shrestha, *Anal. Biochem.*, 2009, **395**, 231-236.
6 S. Effkemann, U. Pinkernell and U. Karst, *Anal. Chim. Acta*, 1998, **363**, 97-103.
7 S. Hanaoka, J. M. Lin and M. Yamada, *Anal. Chim. Acta*, 2001, **426**, 57-64.
8 K. Thenmozhi and S. S. Narayanan, *Sens. Actuator B- Chem.*, 2007, **125**, 195-201.
9 Z. Wang, H. Song, H. Zhao and Y. Lv, *Luminescence*, 2013, **28**, 259-264.
10 S. Chen, R. Yuan, Y. Chai and F. Hu, *Microchim. Acta*, 2013, **180**, 15-32.
11 X. Chen, G. Wu, Z. Cai, M. Oyama and X. Chen, *Microchim. Acta*, 2014, **181**, 689-705.
12 C. Welch, C. Banks, A. Simm and R. Compton, *Anal. Bioana.l Chem.*, 2005, **382**, 12-21.
13 Y. Wang, J. Chen, C. Zhou, L. Zhou, Y. Kong, H. Long and S. Zhong, *Electrochim. Acta*, 2014, **115**, 269-276.
14 Z. Peng and H. Yang, *Nano. Today*, 2009, **4**, 143-164.
15 A. M. Golsheikh, N. M. Huang, H. N. Lim, R. Zakaria and C. Y. Yin, *Carbon*, 2013, **62**, 405-412.
16 V. C. Tung, M. J. Allen, Y. Yang and R. B. Kaner, *Nat. Nanotechnol.*, 2009, **4**, 25-29.
17 W. Liu, J. Zhang, C. Li, L. Tang, Z. Zhang and M. Yang, *Talanta*, 2013, **104**, 204-211.
18 Y. Liang, D. Wu, X. Feng and K. Müllen, *Adv. Mater.*, 2009, **21**, 1679-1683.
19 S. Zhang, Y. Shao, H. Liao, M. H. Engelhard, G. Yin and Y. Lin, *ACS Nano.*, 2011, **5**, 1785-1791.
20 Z. G. Le, Z. Liu, Y. Qian and C. Wang, *Appl. Surf. Sci.*, 2012, **258**, 5348-5353.
21 W. J. Hummers and R. E. Offeman, *J. Am. Chem. Soc.*, 1958, **80**, 442.
22 B. KumaráBarman and K. KaráNanda, *Chem. Commun.*, 2013, **49**, 8949-8951.
23 R. S. Dey, and C. R. Raj, *Biosens. Bioelectron.*, 2014, **62**, 357-364.
24 R. S. Dey, S. Hajra, R. K. Sahu, C. R. Raj and M. K. Panigrahi, *Chem. Commun.*, 2012, **48**, 1787-1789.
25 G. Wang, X. Shen, B. Wang, J. Yao and J. Park, *Carbon*, 2009, 47, 1359–1364.
26 H. C. Schniepp, J. L. Li, M. J. McAllister, H. Sai, M. Herrera-Alonso and D. H. Adamson, *J. Phys. Chem. B*, 2006, **110**, 8535-8539.
27 J. Shi, R. Nie, P. Chen and Z. Hou, *Cata.l Commun.*, 2013, **41**, 101-105.
28 B. Kaur, T. Pandiyan, B. Satpati and R. Srivastava, *Colloids Surf. B-Biointerfaces*, 2013, **111**, 97-106.
29 J. Zhang, H. Yang, G. Shen, P. Cheng, J. Zhang and S. Guo, *Chem. Commun.*, 2010, **46**, 1112-1114.
30 D. Miao, J. Li, R. Yang, J. Qu, L. Qu and Pd. B. Harrington , *J. Electroanal. Chem.*, 2014, **732**, 17-24
31 R. SundaráDey and C. RetnaáRaj, *Chem. Commun.*, 2012, **48**, 1787-1789.
32 M. Zhang, J. Xie, Q. Sun, Z. Yan, M. Chen and J. Jing, *Int. J. Hydrogen Energy*, 2013, **38**, 16402-16409.
33 J. Chen, J. Liu, X. Sun and Y. Chen, *Introduction to Nanomaterials Science*, Higher Education Press, Beijing, 2010.
34 J. Li, Q. Yu and T. Peng, *Anal. Sci.*, 2005, **21**, 377-381.
35 I. Katsounaros, W. B. Schneider, J. C. Meier, U. Benedikt, P. U. Biedermann and A. A. Auer, *Phys. Chem. Chem. Phys.*, 2012, **14**, 7384-7391.
36 X. Zhu, I. Yuri, X. Gan, I.Suzuki and G. Li, Biosens. Bioelectron., 2007, **22**, 1600-1604.
37 C. Shan, H. Yang, D. Han, Q. Zhang, A. Ivaska and L. Niu, *Biosens. Bioelectron.*, 2010, **25**, 1070-1074.
38 X. Liu, X. Xu, H. Zhu and X. Yang, *Anal. Methods*, 2013, **5**, 2298-2304.
39 X. Liu, H. Zhu and X. Yang, *Talanta*, 2011, **87**, 243-248.
40 Q. Wang, M. Li, S. Szunerits and R. Boukherroub, *Electroanalysis*, 2014, **26**, 156-163.
41 Z. Sun, H. Fu, L. Deng and J. Wang, *Anal. Chim. Acta*, 2013, **761**, 84-91.
42 Y. Fang, D. Zhang, X. Qin, Z. Miao, S. Takahashi and J. Anzai, *Electrochim. Acta*, 2012, **70**, 266-271.
43 Q. Xi, X. Chen, D. G. Evans and W. Yang, *Langmuir*, 2012, **28**, 9885-9892.
44 X. M. Chen, Z. X. Cai, Z. Y. Huang, M. Oyama, Y. Q. Jiang and X. Chen, *Electrochim. Acta*, 2013, **97**, 398-403.
45 X. Li, Y. Liu, L. Zheng, M. Dong, Z. Xue, X. Lu and X. Liu, *Electrochim. Acta*, 2013, **113**, 170-175.
46 X. Li, X. Liu, W. Wang, L. Li and X. Lu, *Biosens. Bioelectron.*, 2014, **59**, 221-226.

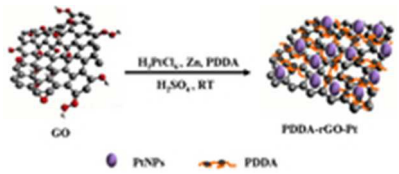

Scheme.1 Schematic illustration of the synthesis procedure of Pt-PDDA-rGO.
16x7mm (300 x 300 DPI)

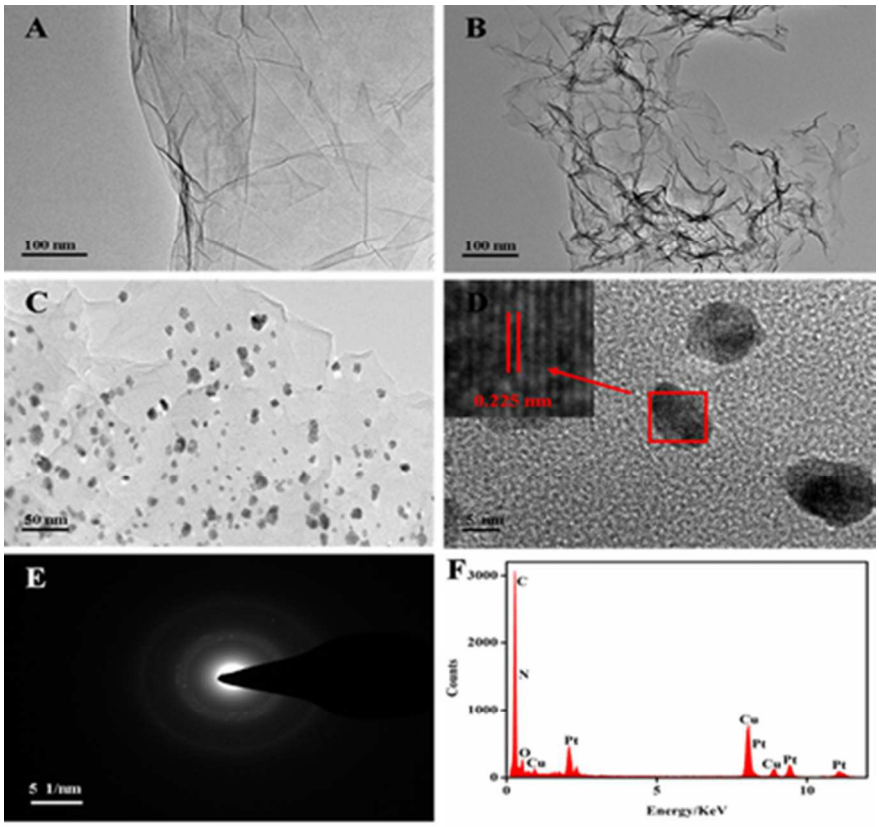

Fig.1 TEM images of the GO (A), PDDA-rGO (B), Pt-PDDA-rGO (C); HRTEM image (D), SAED pattern (E) and the EDX (F) of Pt-PDDA-rGO hybrid material.
36x34mm (300 x 300 DPI)

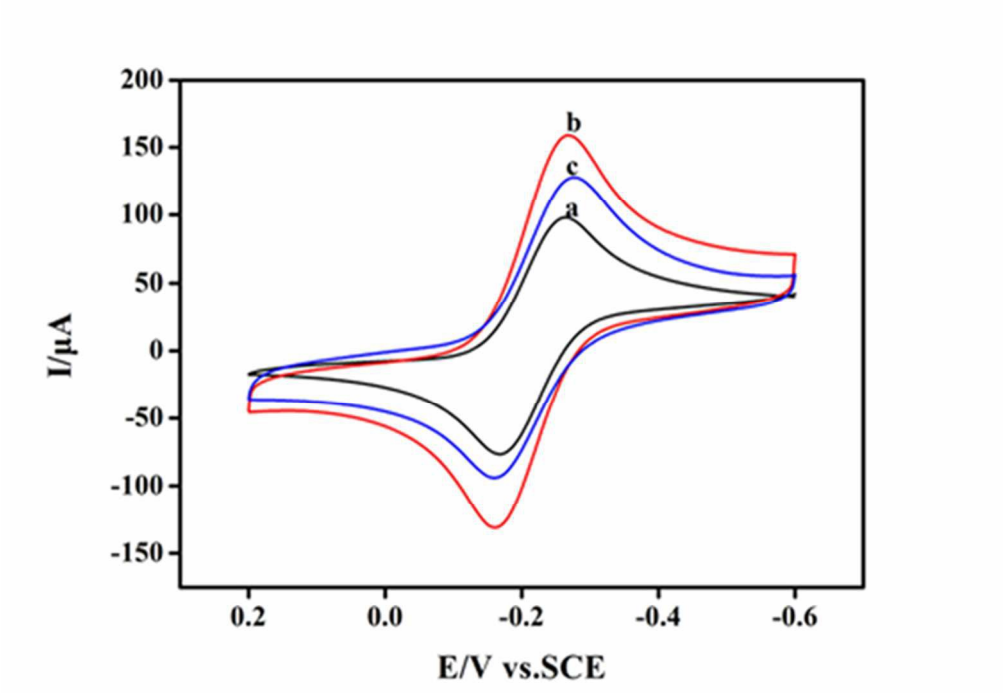

Fig.2 CVs of bare GCE (a), PDDA-rGO/GCE (b), and Pt-PDDA-rGO/GCE (c) in the 10 mM Ru(NH3)63+ and 0.1M KCl solution, at 50 mV/s.
27x19mm (600 x 600 DPI)

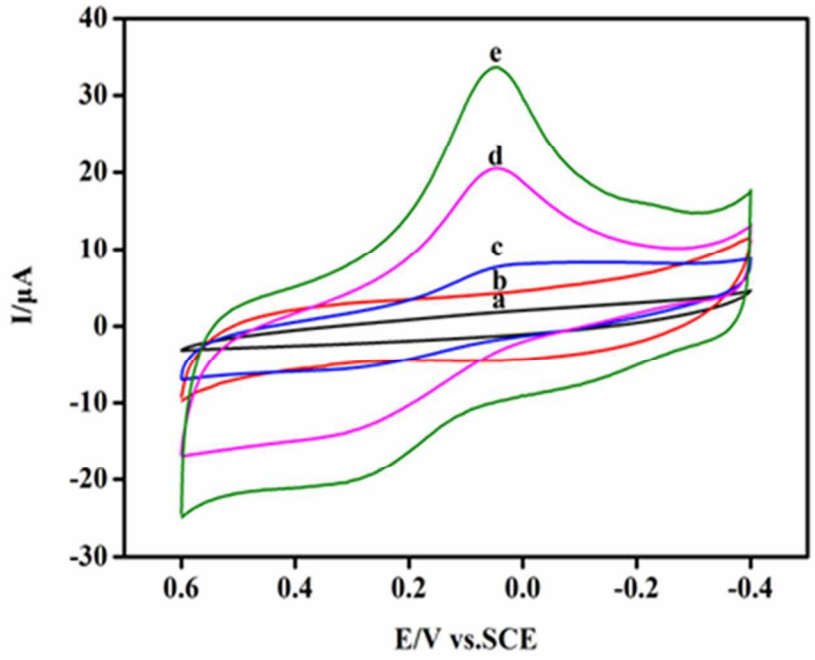

Fig.3 CVs of bare GCE (a), PDDA-rGO/GCE (b), Pt-rGO/GCE (c), Pt-PDDA/GCE (d), and Pt -PDDA-rGO/GCE (e) in the solution of N2-saturated 0.2 M PBS (pH 7.0), at 50 mV/s.
29x22mm (600 x 600 DPI)

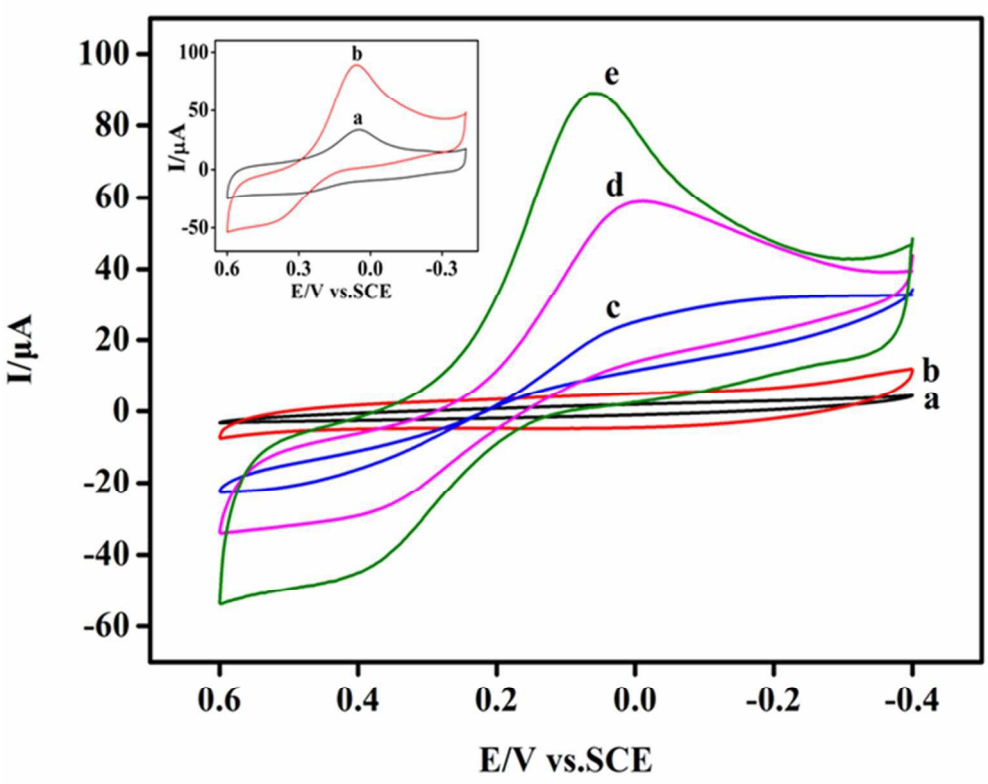

Fig.4 CVs of bare GCE (a), PDDA-rGO/GCE (b), Pt-rGO/GCE (c), Pt-PDDA/GCE(d), and Pt-PDDA-rGO/GCE (e) in the solution of 2.0 mM H_2O_2 and N_2-saturated 0.2 M PBS (pH 7.0). Inset is the CVs of Pt-PDDA-rGO/GCE in N_2-saturated 0.2 M PBS (pH 7.0) without (a) and with (b) 2 mM H_2O_2. Scan rate: 50 mV/s.
30x24mm (600 x 600 DPI)

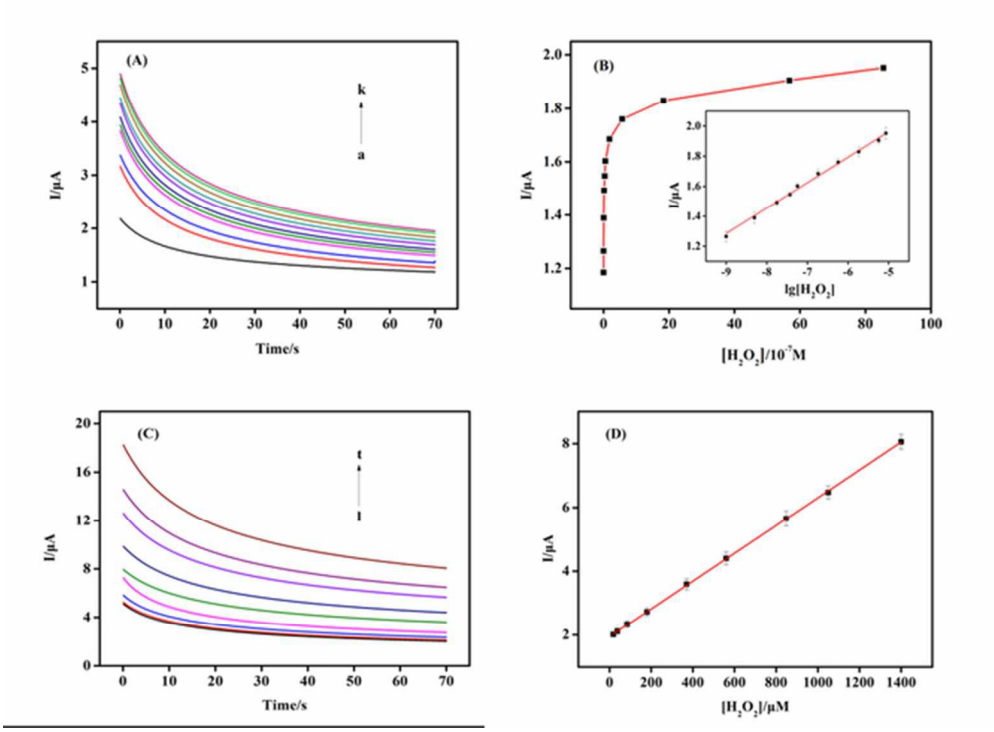

Fig.5 (A) The chronoamperometry current-time curves of Pt-PDDA-rGO/GCE in N2-saturated 0.2 M PBS (pH 7.0) containing various concentrations of H2O2 (from a to k: 0, 1.0×10-9, 5.0×10-9, 1.8×10-8, 3.7×10-8, 5.7×10-8, 1.8×10-7, 5.7×10-7, 1.8×10-6 and 5.7×10-6, 8.6×10-6 M), at 0 V; (B) Relationship between the concentrations of H2O2 and electrocatalytic currents, and the inset is the linear relationship between peak currents and lg[H2O2]; (C) The chronoamperometry current-time curve of Pt-PDDA-rGO /GCE with successive addition of H2O2 (from i to t: 1.8×10-5, 3.7×10-5, 8.5×10-4, 1.8×10-4, 3.7×10-4, 5.6×10-4, 8.5×10-4, 1.1×10-3, 1.4×10-3 M) to N2-saturated 0.2 M PBS (pH 7.0) at 0 V; (D) The calibration plots illustrating the linear electrode response to H2O2 addition.
28x20mm (600 x 600 DPI)

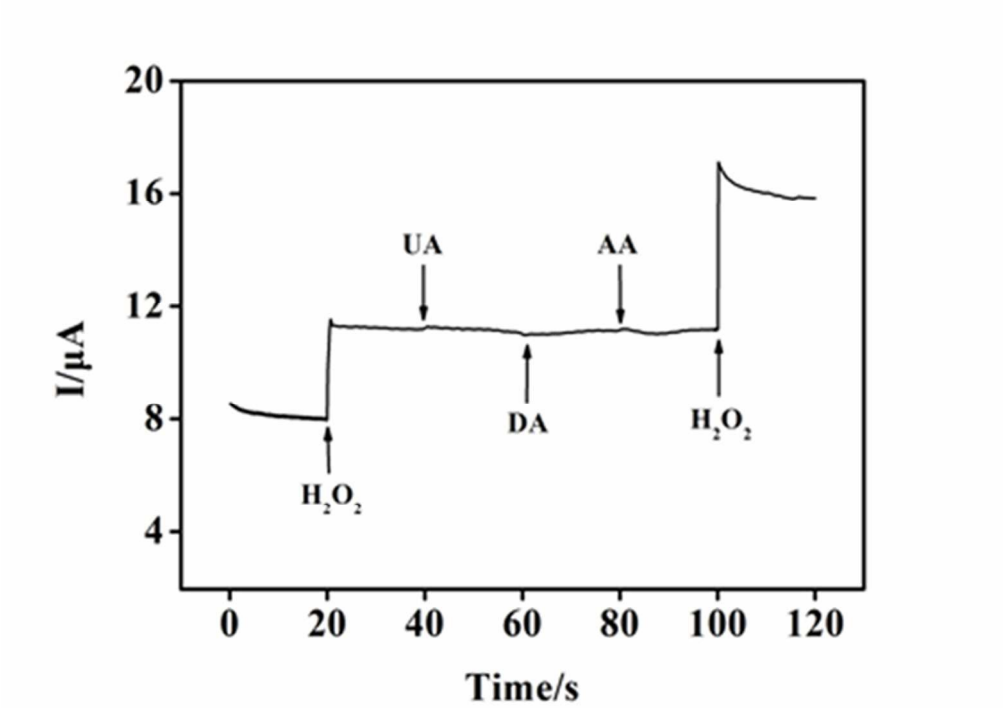

Amperometric i-t response of the Pt-PDDA-rGO/GCE upon the successive addition of H2O2, UA, DA, AA and H2O2 (0.1mM, respectively) into 0.2 M N2-saturated PBS (pH 7.0) at an applied potential of 0 V with stirring condition.
27x19mm (600 x 600 DPI)

Table 1 Comparison of various H_2O_2 sensors.

Electrode	Linear range(μM)	Detection limit(μM)	Ref.
Graphene/AuNPs/chitosan/GCE	200-4200	-	[37]
AgNPs/PDDA/rGO	100-41000	35	[38]
PDDA-G/ Fe_3O_4 /ITO	20-6250	2.5	[39]
rGO/Tyr/GCE	100-2100	80	[40]
Thionine-graphene/GCE	50-1120	18	[41]
PVA-MWCNTs-PtNPs/GCE	2.0-3800	0.7	[42]
AuEPG	0.5-4900	0.1	[43]
PdNPs/rGO	0.1-1000	0.05	[44]
AgNPs/MWCNTs-IL/GCE	0.012-4.8	0.0039	[45]
PtNPs/MWCNTs-SDS/GCE	0.0058-5	0.0019	[46]
	13-1100		
Pt-PDDA-rGO/GCE	0.001-8.6	0.00034	This work
	18-1400		

Table 2 Determination of H_2O_2 in human serum samples.

sample	Added (nM)	Found (nM)	Recovery (%)
1	0	15.58	
2	10	9.51	95.1%
3	20	19.68	98.4%
4	30	30.12	100.4%

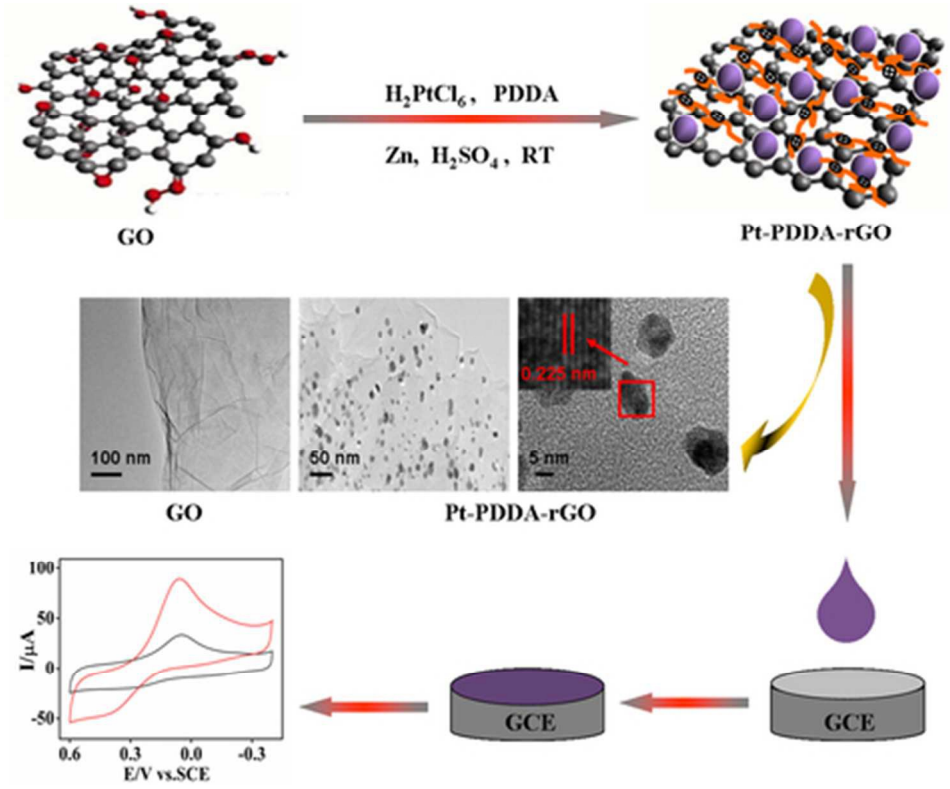

39x33mm (300 x 300 DPI)